This article has been accepted for publication in a future issue of this journal, but has not been fully edited. Content may change prior to final publication. Citation information: DOI 10.1109/LEMCPA.2020.3034759, IEEE Letters on Electromagnetic Compatibility Practice and Applications

IEEE EMC SOCIETY | Letters on Electromagnetic Practice and Applications

A General Method to Calculate the Source-Stirred Correlations in a Well-Stirred Reverberation Chamber

Qian Xu, *Member, IEEE*, Lei Xing, *Member, IEEE*, Yongjiu Zhao, Feng Fang, Tianyun Jia, Chaoyun Song, Yi Huang, *Senior Member, IEEE*

***Abstract*—To identify the independent sample number in a platform-stirred reverberation chamber, the correlated angle of a rotating platform has to be identified. A general numerical method is proposed to calculate the farfield correlation in a source-stirred reverberation chamber. The proposed method is verified using a dipole antenna which has an analytical solution. General source antenna configurations are also investigated (e.g. a Vivaldi antenna) which show that the correlated angle is not sensitive to the radiation pattern of the source-stirred antenna for a large rotating radius.**

***Index Terms*—correlation, radiation pattern, reverberation chamber, source stirring technique.**

I. Introduction

The source stirring technique in a reverberation chamber (RC) has been investigated for years and has been widely applied in EMC and over-the-air (OTA) measurements [1]-[15]. If a Tx or Rx antenna is mounted on a rotating platform (which is named platform stirring), the correlated angle can be measured using a vector network analyzer (VNA) [16]-[19]. From a simulation perspective, analytical results can be obtained under certain conditions [20]. To optimize the source-stirring antenna setup, it is necessary to calculate the correlations among different antenna configurations, thus a general method is required.

In this paper, based on the equivalency between the correlation of the measured *S*-parameters and the radiation patterns [16]-[19], the correlations between two arbitrary radiation patterns can be calculated. This method is a general method and can be applied to arbitrary antenna radiation patterns and arbitrary source stirring configurations. In the source-stirring process, the new position of a stirring antenna means the radiation pattern is transformed into a new coordinate system while the shape of the pattern is kept invariant. Here we do not consider the nonideal effects in an RC such as the insufficient number of modes or the mechanical stirring of the antenna structure or holder [21].

The paper is organized as follows: the method is presented in Section II and validated using an analytical equation. Different configurations are investigated in Section III using a dipole antenna and a Vivaldi antenna. Conclusions are finally summarized in Section IV.

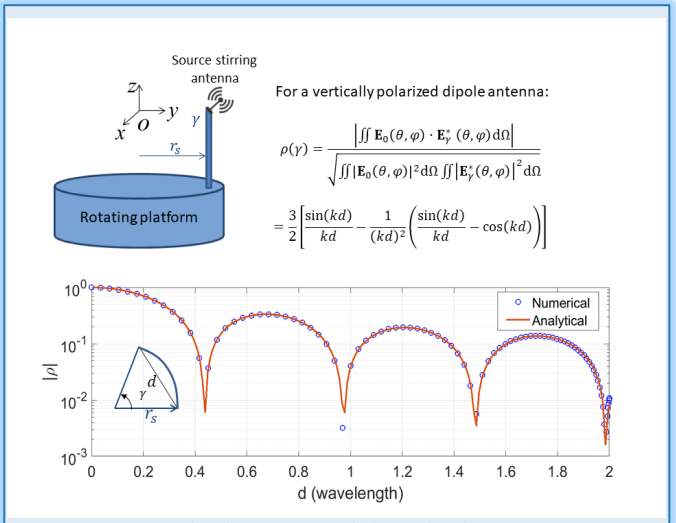

Source stirred antenna correlation (Visual Summary)

II. Numerical Method

A schematic plot of a rotating platform in an RC is illustrated in Fig. 1(a), the origin of the global coordinate system is located at the center of the platform. Suppose the radiation pattern of a rotated antenna is $\mathrm{E}_\gamma(\theta,\varphi)$ in the global coordinate system. To obtain $\mathrm{E}_\gamma(\theta,\varphi)$ in Fig. 1(b), we need to shift the coordinate system in $-y$ direction with a distance r_s and rotate the *xoy* plane with an angle of γ.

Take-Home Messages:

(up to seven items)

- Based on the equivalency between the correlation of the measured *S*-parameters and the radiation patterns, we propose a general method to calculate the source stirred correlation coefficients.
- Without simulating *S*-parameters in a complex cavity directly, the upper bound of the independent sample number can be obtained from the pattern correlations.
- The proposed method can be applied to arbitrary source stirred scenarios and could be used for optimizing the measurement setup.
- The directivity of an antenna does not dominate the correlated angle significantly.

Q. Xu, L. Xing, Y. Zhao and F. Fang are with College of Electronic and Information Engineering, Nanjing University of Aeronautics and Astronautics, Nanjing, 211106, China, E-mail: emxu@foxmail.com, Corresponding author: *Qian Xu*.
C. Song is with the School of Engineering and Physical Sciences, Heriot-Watt University, Edinburgh EH14 4AS, Scotland, UK (e-mail: C. Song@hw.ac.uk).
T. Jia and Y. Huang are with Department of Electrical Engineering and Electronics, The University of Liverpool, Liverpool, L69 3GJ, United Kingdom, E-mail: yi.huang@liverpool.ac.uk.

This article has been accepted for publication in a future issue of this journal, but has not been fully edited. Content may change prior to final publication. Citation information: DOI 10.1109/LEMCPA.2020.3034759, IEEE Letters on Electromagnetic Compatibility Practice and Applications

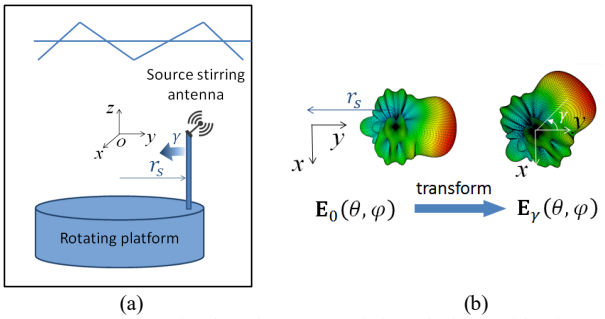

(a) (b)

Figure 1. (a) A schematic plot of a source-stirring platform (side view), the source-stirring antenna is located at (0, r_s, 0), (b) a rotated version of the radiation pattern of a source-stirring antenna (top view). θ is the polar angle, φ is the azimuth angle and γ is the angle of rotation.

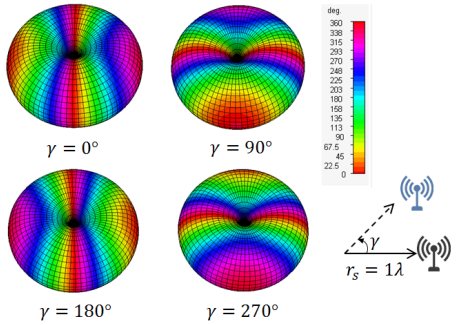

Figure 2. The phase distributions of a rotated dipole antenna ($\angle E_\theta(\theta,\varphi)$) when $\gamma = 0°, 90°, 180°$ and $270°$ in a global coordinate system, the radius of the rotating platform is one wavelength ($r_s = 1\lambda$).

Figure 2 shows a demonstration of the radiation patterns of a rotated dipole with $r_s = 1\lambda$; note that for a z-polarized dipole antenna, the shape of the radiation pattern is not changed but the phase distribution of $E_\theta(\theta,\varphi)$ varies for different angle of rotation γ.

We denote the original radiation pattern as $\mathbf{E}_0(\theta,\varphi)$ (when $\gamma = 0$) and the rotated version as $\mathbf{E}_\gamma(\theta,\varphi)$. In a well stirred RC (isotropic rich multipath environment), from the equivalency between the farfield correlation and the measured S-parameters [16]-[19], the correlation of a platform-stirring antenna can be calculated from

$$\rho(\gamma) = \frac{\left|\iint \mathbf{E}_0(\theta,\varphi)\cdot\mathbf{E}_\gamma^*(\theta,\varphi)\mathrm{d}\Omega\right|}{\sqrt{\iint|\mathbf{E}_0(\theta,\varphi)|^2\mathrm{d}\Omega\iint\left|\mathbf{E}_\gamma^*(\theta,\varphi)\right|^2\mathrm{d}\Omega}} \quad (1)$$

where $\iint \blacksquare \mathrm{d}\Omega = \int_0^{2\pi}\int_0^{\pi} \blacksquare \sin\theta\,\mathrm{d}\theta\,\mathrm{d}\varphi$ represents the integral over solid angle. In an RC, (1) cannot be measured directly as the radiation pattern cannot be measured directly in an RC. However, the S-parameters can be collected to calculate the correlation, and the correlation is the same as (1) in an ideal Rayleigh channel. By calculating (1) numerically (using Matlab), the correlations can be obtained for arbitrary source stirring antennas.

Specifically, when an electrically small dipole is z-polarized (vertically polarized), from the random plane-wave model, the correlation for the transverse E-field with a distance d has been derived in [20] as

$$\rho_t(d) = \frac{3}{2}\left[\frac{\sin(kd)}{kd} - \frac{1}{(kd)^2}\left(\frac{\sin(kd)}{kd} - \cos(kd)\right)\right] \quad (2)$$

where $k = 2\pi/\lambda$ is the wave number. (2) can be used to verify (1) by substituting $d = 2r_s\sin(\gamma/2)$ into (2). Figure 3 shows a comparison between the correlations obtained from the pattern integration in (1) and the random plane-wave model in (2). Experimental validations

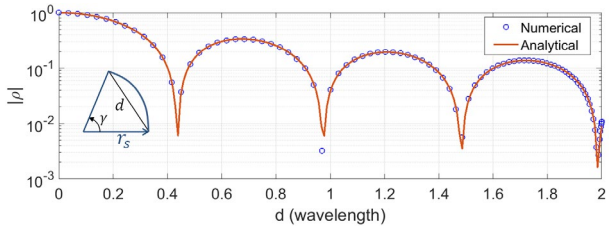

Figure 3. Farfield correlations of a dipole antenna calculated numerically and analytically, a z-polarized dipole is used with a radius of rotation of one wavelength; when $d \approx 0.4367\lambda$, a null is obtained.

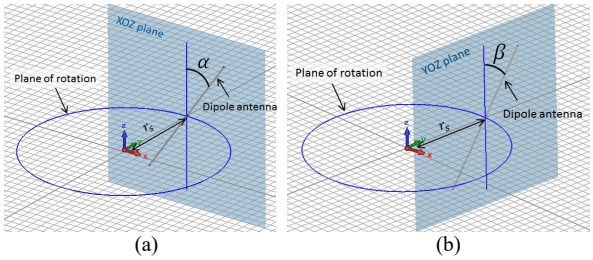

(a) (b)

Figure 4. (a) Definition of α, (b) definition of β, the platform-stirred dipole antenna is located at $(0, r_s, 0)$.

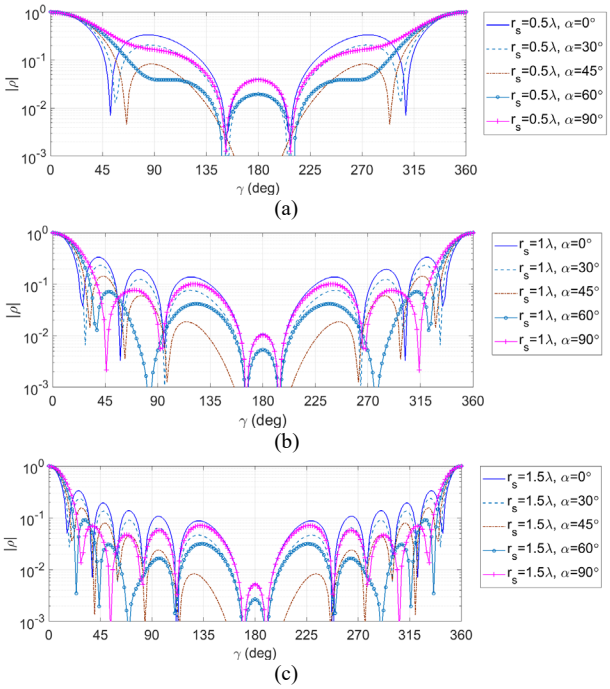

(a) (b) (c)

Figure 5. Farfield correlations for different α (while $\beta = 0$) and different r_s, (a) $r_s = 0.5\lambda$, (b) $r_s = 1\lambda$ and (c) $r_s = 1.5\lambda$.

have also been given in [20]. Considering the efficiency and accuracy in the radiation pattern discretization, a resolution of 2° is used for θ, φ and γ angles in the pattern discretization and transformation, the Simpson's 2D rule is adopted to calculate (1). The numerical error of the Simpson's 2D rule is $O(\Delta\theta^4) + O(\Delta\varphi^4)$ which is very small. In Fig. 3, it should be noted that the distance is not half-wavelength for the first null, because the antenna is z-polarized, the total vector E-field correlation $\sin(kd)/(kd)$ [20] cannot be applied.

III. Simulation Results

To investigate the dependency of the radiation pattern on the platform-stirring correlation, the radiation pattern of a dipole antenna is analyzed with different angles. The position of the antenna is located

This article has been accepted for publication in a future issue of this journal, but has not been fully edited. Content may change prior to final publication. Citation information: DOI 10.1109/LEMCPA.2020.3034759, IEEE Letters on Electromagnetic Compatibility Practice and Applications

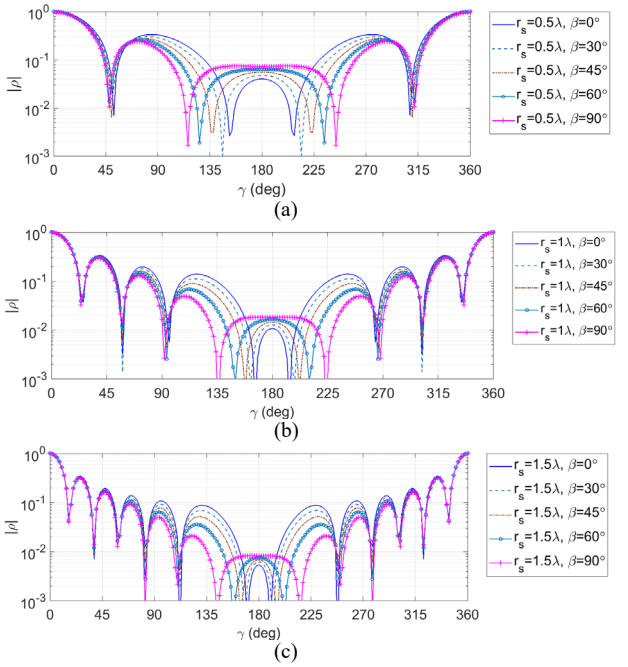

Figure 6. Farfield correlations for different β (while $\alpha = 0$) and different r_s, (a) $r_s = 0.5\lambda$, (b) $r_s = 1\lambda$ and (c) $r_s = 1.5\lambda$.

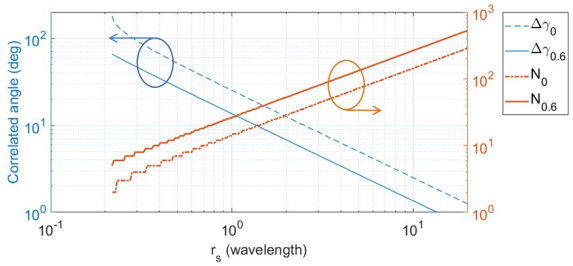

Figure 7. Correlated angles for threshold values of 0 (first null) and 0.6 with different radius of rotation; the dipole antenna is z-polarized.

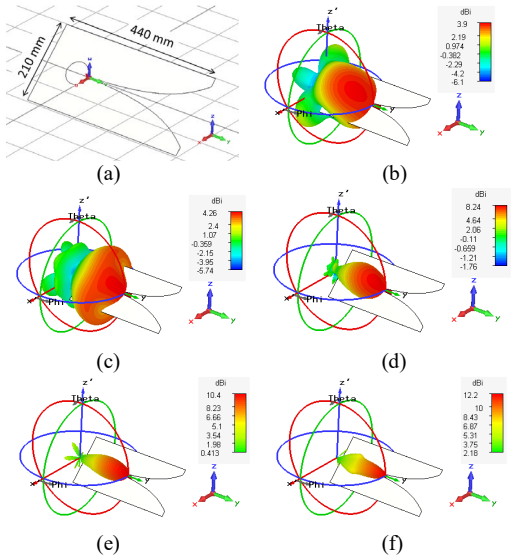

Figure 8. (a) Vivaldi antenna, a tilted angle of $\alpha = 45°$ is used; simulated radiation patterns with a maximum directivity of (b) 3.9 dB @ 0.5 GHz, (c) 4.3 dB @ 1 GHz, (d) 8.2 dB @ 2 GHz, (e) 10.4 dB @ 3 GHz and (f) 12.2 dB @ 5 GHz respectively.

at $(0, r_s, 0)$, where r_s is the radius of rotation. We investigate the angles tilted in two directions in Fig. 4: α angle with z-axis rotated in xoz plane (around y-axis) and β angle with z-axis rotated in yoz plane

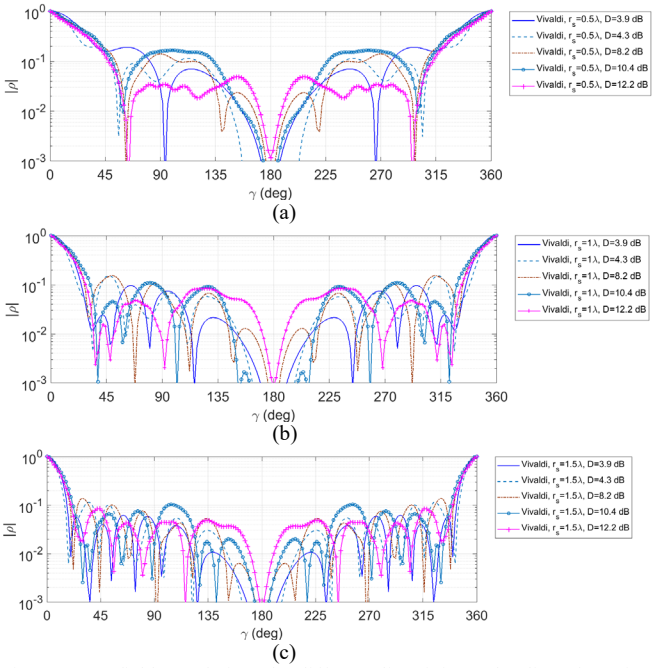

Figure 9. Farfield correlations for different directivity and radius of rotation, (a) $r_s = 0.5\lambda$, (b) $r_s = 1\lambda$ and (c) $r_s = 1.5\lambda$.

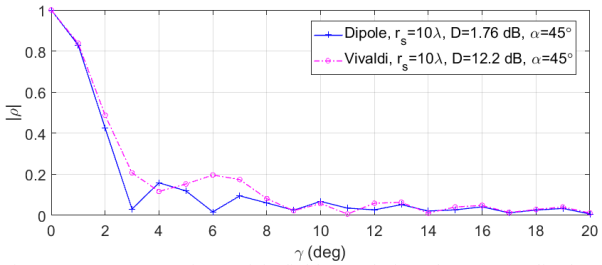

Figure 10. A comparison of farfield correlations between a dipole antenna and a Vivaldi antenna when $r_s = 10\lambda$. 1°/step is used for θ, φ and γ angles respectively.

(around x-axis). The calculated correlations with different r_s, α and β for a dipole antenna are illustrated in Fig. 5 and Fig. 6.

It is interesting to note that the correlations are more sensitive for α angles than β angles for a dipole antenna. When the antenna is z-polarized, the first null is small but the second peak of the correlation is high. It would be useful to find a trade-off between the first null and the envelope of the correlations. (e.g. from Fig. 5, $\alpha = 45°$ or $60°$ could be a good choice.) Note that in the IEC standard, the correlation is defined using received power and a threshold of $1/e \approx 0.37$ is normally used [22]. While for complex S-parameter or radiation pattern correlations, the threshold becomes $\sqrt{1/e} \approx 0.6$ [23], [24]. The angles for the first null and a threshold of 0.6 are presented in Fig. 7 for a z-polarized dipole antenna. The independent sample number is also estimated using $N = 360/\Delta\gamma$. It can be found that when a relatively high threshold is used (e.g. 0.6), the difference of correlated angles (independent sample numbers) is negligible.

A more general scenario is investigated in Fig. 8, a wideband Vivaldi antenna is simulated at different frequencies. Since the directivity of the radiation pattern is function of frequency, we can study the dependency of the directivity on the pattern correlations. After normalizing r_s to the wavelength, the radiation pattern correlations are calculated and summarized in Fig. 9. It can be seen

that the correlations do not show significant dependencies on the directivity of the radiation pattern for a threshold of 0.6. If we compare Fig. 9 with Fig. 5, it can be found that the value of the ratio r_s/λ is fundamental: for small values of the ratio r_s/λ, the correlated angle shows dependency on the radiation pattern, while the higher r_s/λ is, the more the correlation is independent of the radiation pattern of the antenna. This is very useful, which means a high directivity antenna is not necessary in a source-stirred RC. In practice, a high directivity antenna could lead some positions for high K-factors when the main beam of the antenna directs to the points of interest [25]. Different scenarios for r_s up to 10λ have also been simulated which show similar phenomenon, a typical plot is given in Fig. 10.

IV. Discussion And Conclusions

We have calculated angular correlations for platform-stirred antennas in different scenarios numerically. The angular correlations of a z-polarized dipole antenna are verified using an analytical equation. General scenarios with a Vivaldi antenna have also been analyzed.

It is interesting to find that the angular correlations only show dependency with the radiation pattern for small rotating radius. While for large rotating radius, the radiation pattern of an antenna does not affect the correlated angles significantly. This shows that the phase redistribution of the radiation pattern in the stirring process contributes similarly to the magnitude redistribution, and Fig. 7 can be used as typical values for general cases.

The numerical method can be applied to arbitrary antennas and arbitrary source-stirred configurations, as we only need to transform the radiation pattern into a new global coordinate system (from a local coordinate system) and calculate the integral numerically. Note that the correlations calculated in this method is in an RC with enough number of random incident plane waves (the RC is well-stirred), thus the numerical values can be considered as the theoretical limits in an ideal RC. In practice, when the RC is not well-stirred, the correlations could be higher than the simulated values.

Acknowledgement

This work was supported in part by the National Natural Science Foundation of China under Grant 61701224 and the Foundation of Science and Technology on Electronic Test & Measurement Laboratory under Grant 6142001190104.

References

[1] Y. Huang, The Investigation of Chambers for Electromagnetic Systems, DPhil Thesis, University of Oxford, 1993.

[2] Y. Huang and D. J. Edwards, "A novel reverberating chamber: source-stirred chamber," IEEE 8th International Conference on Electromagnetic Compatibility, Edinburgh, pp. 120-124, 1992.

[3] G. Cerri, V. M. Primiani, S. Pennesi and P. Russo, "Source stirring mode for reverberation chambers," IEEE Transactions on Electromagnetic Compatibility, vol. 47, no. 4, pp. 815-823, Nov. 2005.

[4] P. -S. Kildal and C. Carlsson, "Detection of a polarization imbalance in reverberation chambers," Microwave and Optical Technology Letters, vol. 34, no. 2, pp. 145-149, 2002.

[5] E. Jackson and D. Zanette, "Stirred source and method of RFI testing," Canada Patent CA2974054C, Oct. 2, 2018.

[6] A. Cozza, "Source correlation in randomly excited complex media," IEEE Antennas and Wireless Propagation Letters, vol. 11, pp. 105-108, 2012.

[7] A. D. Leo, G. Cerri, P. Russo and V. M. Primiani, "Experimental validation of an analytical model for the design of source-stirred chambers," IEEE Transactions on Electromagnetic Compatibility, vol. 60, no. 2, pp. 540-543, Apr. 2018.

[8] A. De Leo, G. Cerri, P. Russo and V. Mariani Primiani, "Experimental comparison between source stirring and mechanical stirring in a reverberation chamber by analyzing the antenna transmission coefficient," International Symposium on Electromagnetic Compatibility (EMC EUROPE), Amsterdam, 2018, pp. 677-682.

[9] G. Cerri, V. M. Primiani, C. Monteverde and P. Russo, "A theoretical feasibility study of a source stirring reverberation chamber," IEEE Transactions on Electromagnetic Compatibility, vol. 51, no. 1, pp. 3-11, Feb. 2009.

[10] V. M. Primiani, P. Russo and G. Cerri, "Design and testing of an antenna system for the source stirring technique in reverberation chambers," Journal of Electromagnetic Waves and Applications, vol. 26, pp. 837-850, 2012.

[11] A. De Leo, V. M. Primiani, P. Russo and G. Cerri, "Numerical analysis of a reverberation chamber: comparison between mechanical and source stirring techniques," International Symposium on Electromagnetic Compatibility - EMC EUROPE, Angers, France, 2017, pp. 1-6.

[12] A. De Leo, V. M. Primiani, P. Russo and G. Cerri, "Low-frequency theoretical analysis of a source-stirred reverberation chamber," IEEE Transactions on Electromagnetic Compatibility, vol. 59, no. 2, pp. 315-324, Apr. 2017.

[13] A. De Leo, V. M. Primiani, P. Russo and G. Cerri, "Optimization techniques for source stirred reverberation chambers," International Symposium on Electromagnetic Compatibility - EMC EUROPE, Wroclaw, 2016, pp. 199-204.

[14] X. Chen, "Scaling factor for turn-table platform stirring in reverberation chamber," IEEE Antennas and Wireless Propagation Letters, vol. 16, pp. 2799-2802, 2017.

[15] X. Chen, W. Xue, H. Shi, L. Wang, S. Zhu and A. Zhang, "Improving field uniformity using source stirring with orbital angular momentum modes in a reverberation chamber," IEEE Microwave and Components Letters, accepted, 2019.

[16] J. Yang, S. Pivnenko, T. Laitinen, J. Carlsson, and X. Chen, "Measurements of diversity gain and radiation efficiency of the eleven antenna by using different measurement techniques," Proc. 4th Eur. Conf. Antennas Propag. (EuCAP), Apr. 2010, pp. 1–5.

[17] X. Chen, P. S. Kildal, and J. Carlsson, "Comparisons of different methods to determine correlation applied to multi-port UWB eleven antenna," Proc. 5th Eur. Conf. Antennas Propag. (EUCAP), Apr. 2011, pp. 1776–1780.

[18] P. Hallbjorner, "Accuracy in reverberation chamber antenna correlation measurements," Proc. Int. Workshop Antenna Technol., Small Smart Antennas Metamater. Appl. (IWAT), Mar. 2007, pp. 170–173.

[19] Q. Xu, Y. Huang, L. Xing, C. Song, Z. Tian, S. S. Aljaáfreh, and M. Stanley, "3-D antenna radiation pattern reconstruction in a reverberation chamber using spherical wave decomposition," IEEE Transactions on Antennas and Propagation, vol. 65, no. 4, pp. 1728-1739, Apr. 2017.

[20] D. A. Hill, Electromagnetic Fields in Cavities: Deterministic and Statistical Theories, Wiley-IEEE Press, USA, 2009.

[21] Q. Xu, L. Xing, Y. Zhao, T. Jia and Y. Huang, "A source stirred reverberation chamber using a robotic arm," IEEE Transactions on Electromagnetic Compatibility, accepted, 2019. doi: 10.1109/TEMC. 2019.2912999.

[22] IEC 61000-4-21, Electromagnetic compatibility (EMC) – Part 4-21: Testing and measurement techniques – Reverberation chamber test methods, IEC Standard, Ed 2.0, 2011-01.

[23] Q. Xu, L. Xing, D. Yan, Y. Zhao, T. Jia and Y. Huang, "Experimental verification of stirrer angular correlation with different definitions in a reverberation chamber," 12th International Symposium on Antennas, Propagation and EM Theory (ISAPE), Hangzhou, China, 2018, pp. 1-5.

[24] F. Monsef, A. Cozza and R. Serra, "Linking lag-1 correlation coefficients between field-related quantities in a reverberation chamber," IEEE Transactions on Electromagnetic Compatibility, accepted, 2019. doi: 10.1109/TEMC.2019.2928177.

[25] C. Lemoine, E. Amador, P. Besnier, J. Floc'h and A. Laisné, "Antenna directivity measurement in reverberation chamber from Rician K-factor estimation," IEEE Transactions on Antennas and Propagation, vol. 61, no. 10, pp. 5307-5310, Oct. 2013.